J Appl Electrochem (2009) 39:1827–1833
DOI 10.1007/s10800-009-9886-2

ORIGINAL PAPER

Effectiveness factor of fast (Fe^{3+}/Fe^{2+}), moderate (Cl_2/Cl^-) and slow (O_2/H_2O) redox couples using IrO_2-based electrodes of different loading

Erika Herrera Calderon · Alexandros Katsaounis · Rolf Wüthrich · Philippe Mandin · György Foti · Christos Comninellis

Received: 18 November 2008 / Accepted: 29 March 2009 / Published online: 18 April 2009

Abstract The effectiveness factor, E_f, (fraction of the electrode surface that participates effectively in the investigated reaction) of fast (Fe^{3+}/Fe^{2+}), moderate (Cl_2/Cl^-) and slow (O_2/H_2O) redox couples has been estimated using IrO_2-based electrodes with different loading. The method of choice was linear sweep voltammetry (measurement of the anodic peak current) for the Fe^{3+}/Fe^{2+} redox couple and steady-state polarization (determination of the exchange current) for the O_2 and Cl_2 evolution reactions. The results have shown that the effectiveness factor depends strongly on the kinetics of the investigated redox reaction. For the Fe^{3+}/Fe^{2+} redox couple, effectiveness factors close to zero (max 4%) have been obtained contrary to the O_2 evolution reaction where effectiveness factors close to 100% can be achieved, all being independent of IrO_2 loading. For the Cl_2 evolution reaction, intermediate values of the effectiveness factor have been found and they decrease strongly, from 100% down to about 60%, with increasing loading.

Keywords DSA® (Ti/IrO_2) electrodes · Fe^{3+}/Fe^{2+} redox couple · Linear sweep voltammetry (LSV) · O_2 and Cl_2 evolution reactions · Effectiveness factor · Relative effectiveness factor

E. H. Calderon · G. Foti (✉) · C. Comninellis
Ecole Polytechnique Fédérale de Lausanne (EPFL),
Institute of Chemical Sciences and Engineering,
CH-1015 Lausanne, Switzerland
e-mail: gyorgy.foti@epfl.ch

A. Katsaounis
Department of Environmental Engineering,
Laboratory of Air Waste Treatment Technology,
Technical University of Crete, Chania GR73100, Greece

R. Wüthrich
Department of Mechanical and Industrial Engineering,
Concordia University, 1455 de Maisonneuve Blvd. West,
Montreal, QC H3G 1M8, Canada

P. Mandin
ENSCP, Laboratoire d'Electrochimie et de Chimie Analytique,
UMR CNRS 7575, 11 rue Pierre et Marie Curie,
75231 Paris cedex 05, France

1 Introduction

In heterogeneous catalysis, the term effectiveness factor has been introduced by Levenspiel [1]. The effectiveness factor, E_f, is defined as the ratio of the apparent reaction rate within a pore and the reaction rate not affected by diffusion.

In electrochemistry, the effectiveness factor was presented for the first time by Coeuret et al. in 1976 [2] for a 3D electrochemical reactor for the recovery of metal ions. These authors define the effectiveness factor as the ratio of the measured electrolytic current and the current obtained with an electrode whose overpotential is maintained constant. Later, Savinell et al. [3] used the effectiveness factor, E_f, for the investigation of dimensionally stable anodes (DSA®) consisting of an electrocatalytic porous coating of few micrometer thickness deposited on a conductive metal base, usually Ti. These electrodes are 3D devices and, in principle, have a large surface area.

In this study, different electrochemical measurements (linear sweep voltammetry and steady-state polarization) on Ti/IrO_2 electrodes with different IrO_2 loading have been performed for the estimation of the effectiveness factor of three redox couples: Fe^{3+}/Fe^{2+}, O_2/H_2O and Cl_2/Cl^-.

These reactions have been used to evaluate the influence of the electrode kinetics on the effectiveness factor, E_f, (i.e. the effective electrode area that indeed participates in the

electrochemical reaction). In case of the O_2/H_2O and Cl_2/Cl^- redox couples, the experimentally obtained E_f values will be compared with those predicted by the analytical approach of overpotential distribution within the porous electrode (see details in the Appendix).

2 Experimental

The Ti/IrO_2 electrodes have been prepared by thermal decomposition of H_2IrCl_6 (99.9% ABCR) at 500 °C in air. The aqueous solution of the precursor (46 mM) was applied by a micropipette inside a circular slot (ø = 15 mm, $h = 0.5$ mm) on a Ti plate (25 × 25 mm) treated previously in boiling 1 M oxalic acid (≥97% Fluka) solution. Four electrodes with different loading ($E_{0.11}$, $E_{0.28}$, $E_{1.81}$ and $E_{4.07}$) have been prepared, where E stands for electrode and the subscript stands for the loading in mg IrO_2 cm^{-2}.

Electrochemical measurements were done in a single-compartment, three-electrode cell (50 ml) made of Teflon using a computer controlled EcoChemie potentiostat (model Autolab® PGSTAT 30), and the Ti/IrO_2 electrodes ($E_{0.11}$, $E_{0.28}$, $E_{1.81}$ and $E_{4.07}$) have been used with an exposed geometric area of 0.78 cm^2 as the working electrode (WE), Pt wire (Goodfellow 99.99%) as the counter electrode (CE) and a mercurous sulfate electrode (MSE: $Hg/Hg_2SO_4/K_2SO_4$sat., Radiometer REF621; 0.64 V vs. SHE) as the reference electrode (RE).

In the experiments with the Fe^{3+}/Fe^{2+} redox couple, linear sweep voltammetric measurements at different scan rates have been performed at 25 °C in an aqueous solution of 50 mM Fe^{3+}/Fe^{2+} + 1 M HCl. For the O_2 evolution and Cl_2 evolution reaction, (quasi)steady-state polarization measurements with a potential scan rate of 5 mV s^{-1} have been performed at 25 °C in aqueous 1 M $HClO_4$ and 1 M HCl, respectively. All solutions were made using ultrapure (Millipore®) water. Potentials are expressed with respect to the mercurous sulfate electrode (MSE) used as a reference electrode.

The specific IrO_2 loading, m_{sp}, the roughness factor, γ_{3D}, calculated with Eq. 1 and the estimated coating thickness, L, calculated with Eq. 2, for the four IrO_2 electrodes are shown in Table 1.

Table 1 Characteristics of the Ti/IrO_2 electrodes used: Specific IrO_2 loading, m_{sp}, three dimensional roughness factor, γ_{3D} (defined in Eq. 1) and estimated coating thickness, L (calculated with Eq. 2)

m_{sp}/mg IrO_2 cm^{-2}	0.11	0.28	1.81	4.07
γ_{3D}/–	11.2	28.4	184	413
L/μm	0.13	0.32	2.1	4.7

$$\gamma_{3D} = a_{sp} \cdot m_{sp} \quad (1)$$

and

$$L = \frac{m_{sp}}{1000 \cdot \rho \cdot (1 - \varepsilon)} \quad (2)$$

where m_{sp} is the specific IrO_2 loading (mg IrO_2 cm^{-2}), a_{sp} is the specific surface area (=101.5 cm^2 mg^{-1} IrO_2) of the coating [3], ρ is the bulk density of IrO_2 (11.7 g cm^{-3}) and ε is the volume fraction of the pores in the coating (–). Calculations were made assuming $\varepsilon = 0.26$, which corresponds to the closest packing of uniform spherical particles.

2.1 Ohmic (IR_u) drop correction

The ohmic drop correction was performed following the method of Shub [4], which allows the estimation of the total uncompensated resistance of a given system. In this method, it is assumed that the experimentally observed overpotential, η (V), at any current is given by:

$$\eta = a + b \ln I + IR_u \quad (3)$$

where a is the Tafel constant (V), b is the Tafel slope (V dec^{-1}), I is the current (A) and R_u is the total uncompensated resistance (Ω) of the system between the working and the reference electrodes, assumed to be constant and independent of current. Derivation of Eq. 3 with respect to the current density yields Eq. 4, from which b and R_u can be obtained by plotting $\frac{d\eta}{dI}$ Vs. I^{-1}:

$$\frac{d\eta}{dI} = \frac{b}{I} + R_u \quad (4)$$

The knowledge of R_u allows the correction of the experimental overpotential by subtracting the ohmic drop IR_u using Eq. 5:

$$\eta_{corr} = \eta - IR_u \quad (5)$$

In the numerical calculation, the derivative $\frac{d\eta}{dI}$ was replaced by the increments $\Delta\eta/\Delta I$ calculated from each pair of two consecutive experimental points.

2.2 Estimation of the effectiveness factor

For the Fe^{3+}/Fe^{2+} redox couple, the effectiveness factor, E_f, of the IrO_2 electrodes with different loading was calculated through linear sweep voltammetric (LSV) measurements using the relation:

$$E_f = \frac{I_{pa}}{\gamma_{3D} \cdot (I_{pa})_{2D}} \quad (6)$$

where I_{pa} is the anodic peak current (A) measured with a three-dimensional electrode of a given loading, γ_{3D} the

three dimensional roughness factor (–) and $(I_{pa})_{2D}$ the theoretical anodic peak current (A) on a polished (two dimensional) electrode calculated with Eq. 7:

$$(I_{pa})_{2D} = (2.69 \times 10^5) n^{3/2} A_g \cdot D_{Fe^{2+}}^{1/2} \cdot C_{Fe^{2+}} \cdot v^{1/2} \quad (7)$$

where n is the number of exchanged electrons (–), A_g is the geometric surface area (cm^2), $D_{Fe^{2+}}$ is the diffusion coefficient of Fe^{2+} ($cm^2\ s^{-1}$), $C_{Fe^{2+}}$ is the concentration of Fe^{2+} (mol cm^{-3}) and v is the scan rate (V s^{-1}). For the calculation of $(I_{pa})_{2D}$ a diffusion coefficient of $D_{Fe^{2+}} = 5.4 \times 10^{-6} cm^2 s^{-1}$, reported for a polished Pt electrode in aqueous medium [5], has been used.

For oxygen and chlorine evolution, the effectiveness was calculated with respect to the Ti/IrO_2 electrode of lowest loading taken as a reference (relative effectiveness factor, E_f^{rel}) using Eq. 8:

$$E_f^{rel} = \frac{(j_0)_{3D}/m_{sp}}{(j_0)_{3D}^{ref}/m_{sp}^{ref}} \quad (8)$$

where $(j_0)_{3D}^{ref}$ and m_{sp}^{ref} are, respectively, the exchange current density and the specific loading of the reference 3D electrode (in the present case, the electrode $E_{0.11}$ with 0.11 mg IrO_2 cm^{-2} specific loading).

3 Results and discussion

3.1 Effectiveness factor of the Fe^{3+}/Fe^{2+} redox couple

Figure 1a–d shows linear sweep voltammograms without IR_u drop correction, obtained with four different electrode loadings and using different scan rates. Figure 2 shows the plot of anodic peak current, I_{pa}, as a function of the square root of scan rate, $v^{1/2}$, for different loadings. It is seen that the $I_{pa}-v^{1/2}$ curves are quasi-independent of loading. This is already an indication that under the investigated conditions, almost exclusively, the 2D surface is involved in the LSV measurements. In fact, calculated with Eq. 6, the experimentally obtained effectiveness factors, E_f, were found in the 0–4% range. This means that the pores of the 3D structure are not accessible for the reaction due to the fast kinetics of this redox couple.

3.2 Effectiveness factor of the oxygen evolution reaction (O_2/H_2O)

Figure 3 shows a typical polarization curve obtained in 1 M $HClO_4$ on the Ti/IrO_2 electrode ($E_{0.11}$) before (curve 1) and after (curve 2) IR_u drop correction using the uncompensated

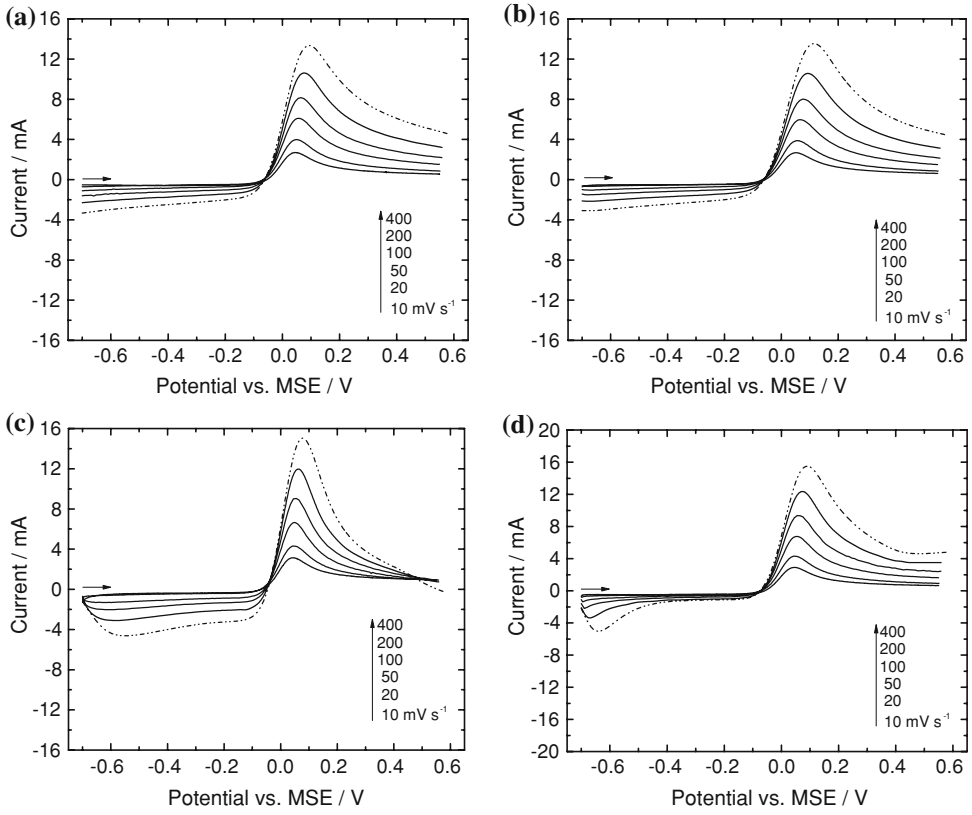

Fig. 1 LSV measurements (without ohmic drop correction) in 50 mM Fe^{3+}/Fe^{2+} + 1 M HCl using four different loadings, **a** $E_{0.11}$, **b** $E_{0.28}$, **c** $E_{1.81}$ and **d** $E_{4.07}$, and different scan rates, 10, 20, 50, 100, 200 and 400 mV s^{-1}. $T = 25$ °C

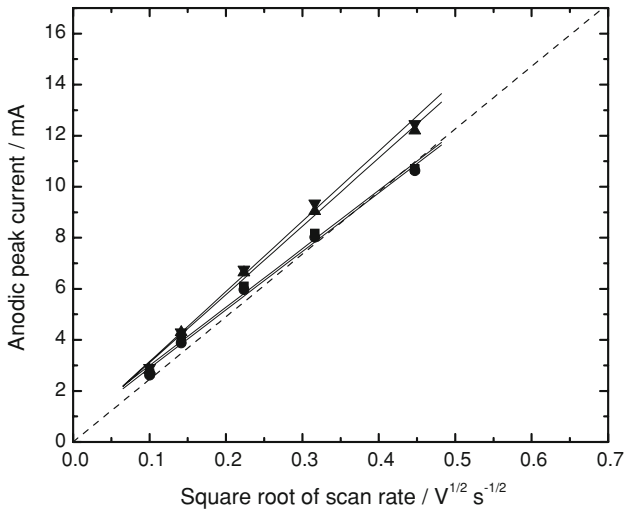

Fig. 2 Anodic peak current, I_{pa}, from measurements of Fig. 1 as a function of the square root of scan rate, $v^{1/2}$, obtained for different electrode loadings: *black square*: $E_{0.11}$, *black circle*: $E_{0.28}$, *black up-pointing triangle*: $E_{1.81}$, *black down-pointing triangle*: $E_{4.07}$. *Dashed line* shows $(I_{pa})_{2D}$ calculated with Eq. 7

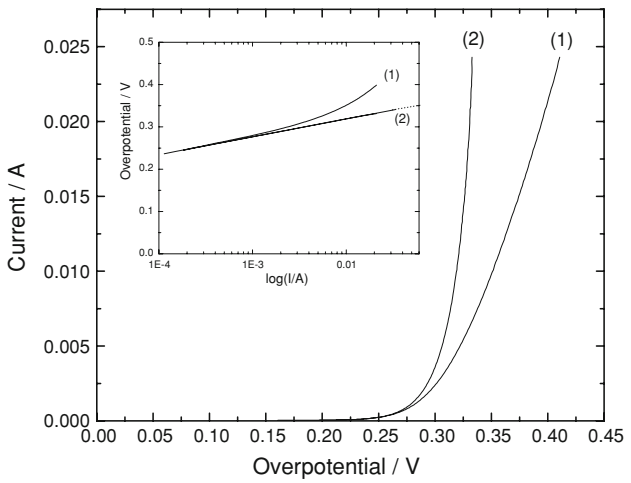

Fig. 3 Steady-state (5 mV s^{-1}) polarization curves obtained in 1 M $HClO_4$ on the Ti/IrO_2 electrode ($E_{0.11}$) before (curve 1) and after (curve 2) ohmic drop correction. Inset: Tafel lines before (curve 1) and after (curve 2) ohmic drop correction. $T = 25$ °C

resistance $R_u(= 3.2\ \Omega)$ of the cell determined from the intersection of the plot of $\Delta\eta/\Delta I$ versus I^{-1} using Eq. 4 (see Fig. 4).

From both the uncorrected and the corrected polarization curves, the Tafel lines were plotted (inset of Fig. 3). It can be seen that in the high overpotential region, the uncorrected curve (curve 1) deviates strongly from linearity. However, the corrected polarization curve (curve 2) is linear, yielding a Tafel slope of 43 mV dec^{-1}.

In acidic medium, the following mechanism for O_2 evolution on oxide electrodes has been proposed [6, 7]:

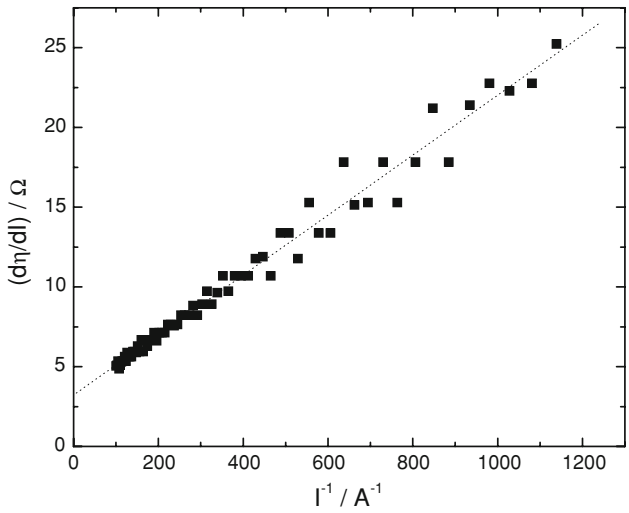

Fig. 4 Determination of the uncompensated resistance from the intersection of the plot of $\Delta\eta/\Delta I$ vs. I^{-1}, using the data of Fig. 3

$$S + H_2O \rightarrow S - OH_{ads} + H^+ + e^- \quad (9)$$

$$S - OH_{ads} \rightarrow S - O_{ads} + H^+ + e^- \quad (10)$$

$$2S - O_{ads} \rightarrow 2S + O_2 \quad (11)$$

In the first step, reaction (9), water is discharged forming adsorbed hydroxyl radicals. These hydroxyl radicals are further discharged forming a higher oxide according to reaction (10), which is finally decomposed to oxygen liberating the active site S following reaction (11).

Depending on the rate-determining step (rds) of this process, different Tafel slopes can be expected: 120 mV dec^{-1} if step 1 is the rds, 40 mV dec^{-1} if step 2 is the rds and 15 mV dec^{-1} if step 3 is the rds. The obtained experimental Tafel slope (43 mV dec^{-1}) indicates that certainly the formation of the higher oxide is the rate-determining step of the process. In fact, using differential mass spectroscopy (DEMS) measurements with $^{18}O_2$, it has been demonstrated that the higher oxide indeed participates in the oxygen evolution reaction [8]. Furthermore, the exchange current density, j_0(mA cm^{-2}), and the Tafel slope, b, of the oxidation of the redox couple O_2/H_2O can be determined using Eq. 3. Table 2 shows the j_0 and b values obtained for the four investigated Ti/IrO_2 electrodes.

The effectiveness factor, E_f, of the Ti/IrO_2 electrodes can be also predicted from an analytical approach (see Eq. 17 and details in the Appendix) and compared with the experimental relative effectiveness factor calculated with Eq. 8. For the prediction, the coating was modelled with close packing of uniform spherical particles ($\varepsilon = 0.26$) having an estimated diameter of 2 nm to give a specific particle area of $a_p = 3 \times 10^{-7}$ cm^{-1}, and a bulk electrolyte conductivity of $\gamma_0 = 0.37\ \Omega^{-1}$ cm^{-1} was considered. Table 3 shows that, as predicted, the experimental relative

Table 2 Exchange current density, j_0, and Tafel slope, b (see Eq. 3), of the O_2/H_2O redox couple for four Ti/IrO_2 electrodes of different specific loading, m_{sp}, and the three dimensional roughness factor, γ_{3D} (defined in Eq. 1)

m_{sp}/mg cm^{-2}	γ_{3D}/–	j_0/mA cm^{-2}*	b/V dec^{-1}
0.11	11.2	1.34×10^{-6}	0.043
0.28	28.4	2.75×10^{-6}	0.043
1.81	184	2.35×10^{-5}	0.043
4.07	413	6.02×10^{-5}	0.043

* Reported for 1 cm^2 geometric (projected) area

Table 3 Oxygen evolution reaction: Comparison of the predicted (see Appendix) and experimental (Eq. 8) relative effectiveness factors, E_f^{rel}, for various IrO_2 loadings

	Prediction		Experimental	
m_{sp}/mg cm^{-2}	K/–	E_f^{rel}/–	$j_{0(3D)}$/mA cm^{-2}*	E_f^{rel}/–
0.11	0.00005	1.00**	1.34×10^{-6}	1.00**
0.28	0.0001	1.00	2.75×10^{-6}	0.81
1.81	0.0008	1.00	2.35×10^{-5}	1.07
4.07	0.0018	1.00	6.02×10^{-5}	1.21

The estimated experimental error of E_f^{rel} is 20%

* Reported for 1 cm^2 geometric (projected) area

** Taken as a reference

effectiveness factors, E_f^{rel}, are close to unity (found between 0.8 and 1.2), indicating that practically the whole active 3D surface of the coating participates in this reaction (so almost 100% of effectiveness factor). Two factors contribute in the obtained high effectiveness factor: The O_2/H_2O reaction is slow (low j_0 value) and there is no concentration gradient within the coating as water is the reactive species present in excess.

3.3 Effectiveness factor of the chlorine evolution reaction (Cl_2/Cl^-)

Figure 5 shows a polarization curve typical for all Ti/IrO_2 electrode loadings obtained in 1 M HCl before and after IR_u drop correction using the uncompensated resistance determined from the intersection of the plot of $\Delta\eta/\Delta I$ versus I^{-1} using Eq. 4. From the corrected polarization curves, the Tafel lines were plotted (inset of Fig. 5) and the exchange current density (for 1 cm^2 geometric area), j_0, of the redox couple Cl_2/Cl^- has been determined using Eq. 3 for the four investigated IrO_2 loadings (Table 4).

The same approaches as those given for O_2 evolution have been used for the estimation of the predicted and experimental relative effectiveness factor, E_f^{rel}. Again, the lowest IrO_2 loading ($E_{0.11}$) has been used as a reference. Table 5 shows that both the predicted and the experimental

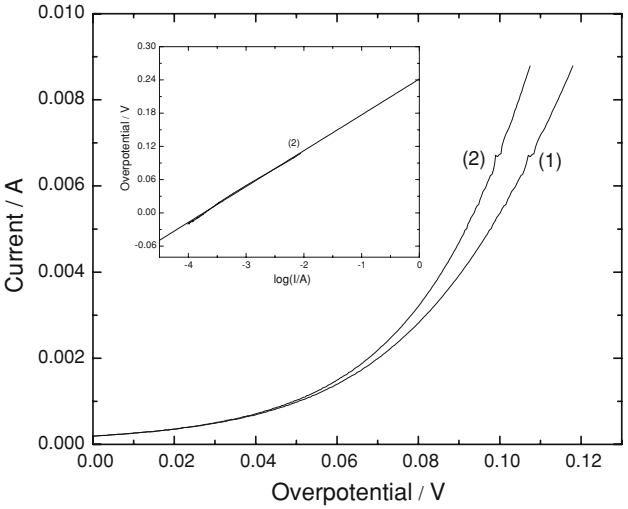

Fig. 5 Steady-state (5 mV s^{-1}) polarization curves obtained in 1 M HCl on the Ti/IrO_2 electrode ($E_{0.11}$) before (curve 1) and after (curve 2) ohmic drop correction. *Inset*: Tafel line after ohmic drop correction (curve 2)

Table 4 Exchange current density, j_0, of the Cl_2/Cl^- redox couple for four Ti/IrO_2 electrodes of different specific loading, m_{sp}, and the three dimensional roughness factor, γ_{3D} (defined in Eq. 1)

m_{sp}/mg cm^{-2}	γ_{3D}/–	j_0/mA cm^{-2}*
0.11	11.2	0.22
0.28	28.4	0.56
1.81	184	2.32
4.07	413	4.83

* Reported for 1 cm^2 geometric (projected) area

Table 5 Chlorine evolution reaction: comparison of the predicted (see Appendix) and experimental (Eq. 8) relative effectiveness factors, E_f^{rel}, for various IrO_2 loadings

	Prediction		Experimental	
m_{sp}/mg cm^{-2}	K/–	E_f^{rel}/–	$j_{0(3D)}$/mA cm^{-2}*	E_f^{rel}/–
0.11	0.019	1.00**	0.22	1.00**
0.28	0.050	1.00	0.56	0.98
1.81	0.32	0.97	2.32	0.64
4.07	0.72	0.86	4.83	0.59

The estimated experimental error of E_f^{rel} is 20%

* Reported for 1 cm^2 geometric (projected) area

** Taken as a reference

relative effectiveness factor decreases with the IrO_2 loading, the latter being found between 1.0 and 0.6 in a reasonable agreement with prediction. Hence, with the Cl_2/Cl^- redox couple, the effectiveness is situated between those with O_2/H_2O and Fe^{3+}/Fe^{2+} redox couples because its kinetics is also intermediate between those of O_2/H_2O and Fe^{3+}/Fe^{2+}.

4 Conclusions

From this study, the following conclusions can be drawn:

- Linear sweep voltammetric (LSV) measurements with the Fe^{3+}/Fe^{2+} redox couple have shown that the I_{pa} vs. $v^{1/2}$ plots are quasi-independent of loading, and effectiveness factors, E_f, in the range of 0 to 4% were obtained. This means that under the investigated conditions, only the 2D electrode surface area of the Ti/IrO_2 electrode is involved in the LSV measurements.
- The investigation of the kinetics of O_2 and Cl_2 evolution shows that chlorine evolution is much faster than oxygen evolution. With the $E_{0.11}$ electrode, exchange current density of 0.22 mA cm^{-2} was found for chlorine evolution, and only 1.3×10^{-6} mA cm^{-2} for oxygen evolution.
- The relative effectiveness factors, E_f^{rel}, for O_2 evolution are close to unity (between 0.8 and 1.2) for all IrO_2 loadings, which show that practically all the 3D surfaces work effectively. However, for the Cl_2/Cl^- redox couple E_f^{rel} values between 0.6 and 1 were found, and they decrease with the IrO_2 loading. Just as its kinetics, the effectiveness factor of the Cl_2/Cl^- redox couple also lies between those of the O_2/H_2O and Fe^{3+}/Fe^{2+} redox couples. The experimentally obtained effectiveness factors for both O_2 and Cl_2 evolution are in reasonably good agreement with the prediction based on the analytical approach.

Acknowledgement The authors acknowledge the *Fonds National Suisse de la Recherche Scientifique* for the financial support.

Appendix: Analytical solution of the effectiveness factor

Coeuret et al. [2] attributed the observed decrease of effectiveness with increasing electrode thickness to an overpotential distribution in the electrolyte within the coating. In order to determine the effectiveness of a DSA® electrode, we have adopted this approach proposed originally for the design of a porous medium for the recovery of heavy metals. As illustrated in Fig. 6, we consider a differential element of thickness, Δx, and cross-section, A_g, and we suppose no concentration gradient in the pores.

Considering that the electronically conductive phase of the coating is equipotential, one can obtain for the overpotential, η, as a function of the dimensionless distance, X, the following second order linear ordinary differential equation:

$$\frac{d^2\eta(X)}{dX^2} - K^2\eta(X) = 0 \tag{12}$$

whose solution is written as

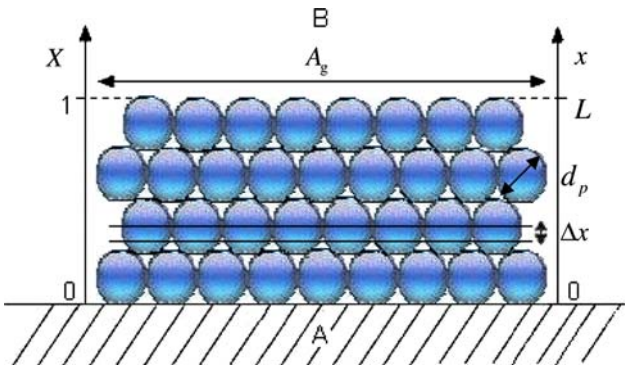

Fig. 6 Schematic representation of the DSA® electrode according to a spherical particle configuration (SPC) consisting of IrO_2 spherical particles with diameter, d_p, showing a differential element of thickness, Δx, and cross-section, A_g. L is the thickness of the coating and X is the dimensionless distance. (a) Ti substrate; (b) electrolyte

$$\frac{\eta(X) - \eta(0)}{\eta(1) - \eta(0)} = \frac{\cosh(KX) - 1}{\cosh(K) - 1} \tag{13}$$

The dimensionless number K^2 includes the morphological parameters like specific particle area, a_p (cm^{-1}), void fraction of the DSA® coating, porosity, ε (–), thickness of the coating, L (cm), the apparent electrolyte conductivity (γ) and the kinetics of the investigated electrochemical reaction (j_0). For spherical particles, the specific area, a_p, is equal to $6/d_p$, where d_p is the particle diameter (cm). The apparent electrolyte conductivity within the DSA® coating, γ, depends on the void fraction, ε, as follows [2]:

$$\gamma = \gamma_0\left(\frac{2\varepsilon}{3 - \varepsilon}\right) \tag{14}$$

where γ is the apparent electrolyte conductivity inside the DSA® coating (Ω^{-1} cm^{-1}), and γ_0 is the bulk electrolyte conductivity (Ω^{-1} cm^{-1}).

Using the low-field approximation of the Butler-Volmer relationship,

$$j = j_0\frac{F}{RT}\cdot\eta \tag{15}$$

where j is the current density (A cm^{-2}), j_0 is the exchange current density (A cm^{-2}), F is the Faraday constant 96485 (C mol^{-1}), R is the molar gas constant 8.31 (J mol^{-1} K^{-1}), T is the temperature (K) and η is the overpotential (V), the parameter K is given by Eq. 16:

$$K^2 = \frac{1}{\gamma}L^2 j_0\frac{F}{RT}(1 - \varepsilon)a_p \tag{16}$$

Finally, the effectiveness factor, E_f, of the DSA® coating can be calculated from K with Eq. 17:

$$E_f = \frac{\tanh(K)}{K} \tag{17}$$

References

1. Levenspiel O (1972) Chemical reaction engineering, 2nd edn. Wiley Eastern Ltd, New Delhi, p 473
2. Coeuret F, Hutin D, Gaunand A (1976) J Appl Electrochem 6:417
3. Savinell RF, Zeller RL, Adams JA (1990) J Electrochem Soc 137:489
4. Shub DM, Reznik MF, Shalaginov VV (1985) Elektrokhimiya 21:937
5. Baticle AM, Perdu F, Vennereau P (1971) Electrochim Acta 16:901
6. De Faria LA, Boodts JFC, Trasatti S (1996) J Appl Electrochem 26:1195
7. Da Silva LM, Boodts JFC, De Faria LA (2001) Electrochim Acta 46:1369
8. Fierro S, Nagel T, Baltruschat H, Comninellis Ch (2007) Electrochem Comm 9:1969